Theory of polarized photoluminescence of indirect band gap excitons in type-I quantum dots

D. S. Smirnov ⊙[*] and E. L. Ivchenko

Ioffe Institute, 194021 St. Petersburg, Russia

In this paper, we theoretically investigate the optical orientation and alignment of excitons in quantum dots with weak electron-hole exchange interaction and long exciton radiative lifetimes. This particular regime is realized in semiconductor heterosystems where excitons are indirect in the r or k space. The main role in the fine structure of excitonic levels in these systems is played by the hyperfine interaction of the electron in the confined exciton and fluctuations of the Overhauser field. Along with it, the effects of nonradiative recombination and exchange interaction are considered. We start with the model of vanishing exchange interaction and nonradiative exciton recombination and then take them into consideration in addition to the strong Overhauser field. In the nano-objects under study, the polarization properties of the resonant photoluminescence are shown to vary with the external magnetic field in a completely different way as compared with the behavior of conventional quantum dot structures.

I. INTRODUCTION

Quantum dots were discovered for the first time in a glass matrix by Ekimov and Onushchenko in 1981 [1], in colloids by Rossetti, Nakahara, and Brus in 1983 [2], and in an ordered semiconductor matrix by Goldstein *et al.* in 1985 [3]. Since then, quantum dots have become one of the central topics in nanotechnology; see, e.g., the reviews in Refs. [4–6] and the books in Refs. [7,8].

Excitons play a dominant role in the optical properties of undoped and weakly doped low-dimensional structures. The fine structure of excitonic levels is crucial for understanding and manipulating these properties. The fine structure of the exciton ground state in semiconductor quantum dots is determined by the splitting of four sublevels formed by the twofold degenerate electron and hole states [9,10]. The nature of the splitting and the oscillator strengths of optical transitions depend on the type of nanostructure. It is convenient to denote the four possible types of quantum dots as d-r–d-k, ind-r–d-k, d-r–ind-k and ind-r–ind-k, where "d" and "ind" stand for *direct* and *indirect* and r and k denote the real and reciprocal spaces. Quantum dots of the d-r–d-k type were the first to be fabricated. Examples include nanocrystal CuCl [1] and CdS [2], as well as InGaAs/GaAs quantum dots fabricated by Stranski-Krastanov growth [4]. The polarized exciton luminescence of this type of quantum dots is well studied [11–15].

The ind-r–d-k quantum dots are composed of two direct band gap semiconductors with the bottom of the conduction band and top of the valence band being located in different materials. As a result, the electron and hole wave functions are concentrated in different regions of the r space, but in the same region of the k space. Examples

of such nanostructures are GaSb/GaAs quantum dots [16] and CdTe/CdSe and CdSe/ZnTe "core-shell" quantum dots [17,18], as well as transition metal dichalcogenide heterobilayers [19–22] and perovskite nanocrystals [23]. The InAlAs/AlGaAs and Ga(As,P)/GaP heterosystems represent ind-r–ind-k-type quantum dots [24,25]; this role can also be played by localized excitons in the GaAs/AlAs superlattice with thin GaAs layers. In such a multilayer structure, an electron in the exciton is localized within the AlAs layer in the X valley of the Brillouin zone, while the hole is localized in the GaAs layer at the center of the Brillouin zone; this is the so-called Γ-X exciton [26–29].

The (In,Al)As/AlAs heteropair represents quantum dots of the fourth type, namely d-r–ind-k [30–32]. Due to the high AlAs potential barrier an electron and a hole are confined within the nanovolume of the (In,Al)As solid solution and also form a Γ-X exciton. Less studied examples of d-r–ind-k quantum dots are provided by GaAs/GaP, InSb/AlAs, and GaSb/AlGaSb heteropairs [33–35] and also effectively by width fluctuations of atomically thin (In,Al)(Sb,As)/AlAs and (Ga,Al)(Sb,As)/AlAs quantum wells [36,37].

Under resonant optical excitation of quantum dots, the exciton spin dynamics is determined by the relation between the following parameters: the exchange interaction energy δ, the radiative and nonradiative decay rates $\hbar/\tau_r$ and $\hbar/\tau_{nr}$, the interaction energy ε_N of the electron with a fluctuation of the nuclear field $\boldsymbol{B}_N$, and the energy ε_B of the Zeeman interaction with an external magnetic field $\boldsymbol{B}$. In ordinary d-r–d-k quantum dots, the exchange interaction exceeds the other parameters, and the role of nuclei is insignificant for neutral excitons. By contrast, for charged quantum dots, the hyperfine interaction is the source of the spin relaxation both in the ground [38–40] and trion states [41,42]. In the GaAs/AlAs superlattice, a localized exciton encompasses a large number of nuclear spins N, and hence the hyperfine interaction $\varepsilon_N \propto N^{-1/2}$ is negligible.

_____
*smirnov@mail.ioffe.ru

In this paper, we theoretically study the optical orientation and alignment of excitons in quantum dots that are indirect in the $\boldsymbol{r}$ or $\boldsymbol{k}$ space. In this case, the reduced overlap of the electron and hole wave functions in the corresponding space suppresses the radiative recombination and the (long-range) exchange interaction making valid the following condition:

$$\varepsilon_N \gg \delta, \frac{\hbar}{\tau_r}, \frac{\hbar}{\tau_{\mathrm{nr}}}. \tag{1}$$

To be specific, we focus on (In,Al)As/AlAs quantum dots, which are the most studied; the generalization for the other systems is straightforward. Our aim is to examine the role of the three small parameters on the right-hand side of the inequalities (1) in polarized exciton photoluminescence (PL) in an external magnetic field $\boldsymbol{B}$.

This paper is structured as follows. In Sec. II, the states of the exciton quadruplet are introduced, their symmetry is analyzed for the point group D_{2d}, and the relationship between the polarizations of the secondary and initial radiation is found in the case of strong splitting between sublevels of the quadruplet. In Sec. III, the simplest model is developed that neglects both the exciton nonradiative recombination and the exchange interaction. In this model, we calculate magnetic field dependences of the degrees of circular and linear polarization of luminescence under polarized photoexcitation. The obtained results serve as a basis for the analysis of the roles of the nonradiative recombination in Sec. IV and the exchange interaction in Sec. V. Section VI discusses and summarizes the obtained results.

II. EXCITON QUADRUPLET

To calculate the PL polarization dependences on the parameters of the system, it is necessary to adopt a certain point symmetry of the quantum dot. For definiteness, we choose the symmetry of the point group D_{2d}. In this case, the electronic Bloch states in the conduction band,

$$\psi_{\frac{1}{2}}^{(e)} = \alpha S, \quad \psi_{-\frac{1}{2}}^{(e)} = \beta S, \tag{2}$$

and hole states in the valence band,

$$\psi_{\frac{1}{2}}^{(h)} = -\beta \frac{\mathcal{X} - i\mathcal{Y}}{\sqrt{2}}, \quad \psi_{-\frac{1}{2}}^{(h)} = \alpha \frac{\mathcal{X} + i\mathcal{Y}}{\sqrt{2}}, \tag{3}$$

transform under the operations of the group D_{2d} according to the equivalent spinor representations Γ_6. Here, $\mathcal{X}, \mathcal{Y}$ are the orbital Bloch functions at the center of the Brillouin zone which transform in D_{2d} as the coordinates $x \parallel [100]$ and $y \parallel [010]$. The electron orbital wave function S mainly belongs to one of the X-valley states, which are Kramers degenerate. The optical properties are determined by its weak and spin-independent mixing with the s-like (Γ_1) orbital of the conduction band at the center of the Brillouin zone [43]. For the ground level of the exciton quadruplet in the quantum dot, we choose the basis of four states Ψ_n ($n = 1$–4) in the form of the following products:

$$\Psi_1 = \psi_{\frac{1}{2}}^{(e)} \psi_{-\frac{1}{2}}^{(h)}, \quad \Psi_2 = \psi_{\frac{1}{2}}^{(e)} \psi_{\frac{1}{2}}^{(h)},$$

$$\Psi_3 = \psi_{-\frac{1}{2}}^{(e)} \psi_{-\frac{1}{2}}^{(h)}, \quad \Psi_4 = \psi_{-\frac{1}{2}}^{(e)} \psi_{\frac{1}{2}}^{(h)}. \tag{4}$$

The two-particle optical excitation of an electron $\psi_s^{(e)}$ and a hole $\psi_{s'}^{(h)}$ is described by the matrix element for the transition from the valence band state $\mathcal{K}\psi_{s'}^{(h)}$ to the conduction band state $\psi_s^{(e)}$, where $\mathcal{K}$ is the time-reversal operator:

$$\mathcal{K}\alpha = \beta, \quad \mathcal{K}\beta = -\alpha, \quad \mathcal{K}(\mathcal{X} \pm i\mathcal{Y}) = \mathcal{X} \mp i\mathcal{Y}. \tag{5}$$

According to Eqs. (2) and (3), due to the spin conservation, the optical excitation of the states Ψ_1, Ψ_4 is forbidden (they are dark), while the states Ψ_2 and Ψ_3 are bright and characterized by the optical matrix elements [7]

$$M_2^{(\mathrm{abs})}(\boldsymbol{e}^{(0)}) = M_0(e_x^{(0)} + ie_y^{(0)}),$$

$$M_3^{(\mathrm{abs})}(\boldsymbol{e}^{(0)}) = M_0(e_x^{(0)} - ie_y^{(0)}), \tag{6}$$

where $\boldsymbol{e}^{(0)}$ is the unit polarization vector of the exciting light. The coefficient M_0 describes the zero-phonon excitation of an electron-hole X-Γ pair; it can be considered real valued. For the nonresonant excitation, the description remains valid provided the spin relaxation during the energy relaxation is negligible. The matrix elements for emission of a photon of the polarization $\boldsymbol{e}$ are related to $M^{(\mathrm{abs})}$ by the relation

$$M_n^{(\mathrm{em})}(\boldsymbol{e}) \propto M_n^{(\mathrm{abs})*}(\boldsymbol{e}) \quad (n = 2, 3).$$

States 1 and 4 are optically dipole inactive [7].

It is useful, instead of basis states 2 and 3, to consider their linear combinations

$$\Psi_x = \frac{1}{\sqrt{2}}(\Psi_2 + \Psi_3), \quad \Psi_y = \frac{i}{\sqrt{2}}(\Psi_2 - \Psi_3), \tag{7}$$

which are optically active in the polarizations $\boldsymbol{e}^{(0)}, \boldsymbol{e} \parallel x$ and $\boldsymbol{e}^{(0)}, \boldsymbol{e} \parallel y$, respectively.

Below we consider the geometry of an experiment where the exciting light and secondary radiation propagate along the structure growth axis z and the light polarization vectors are lateral,

$$\boldsymbol{e}^{(0)} = (e_x^{(0)}, e_y^{(0)}, 0), \quad \boldsymbol{e} = (e_x, e_y, 0). \tag{8}$$

Then the components of the polarization density matrices of the incident and emitted light, $d_{\alpha,\beta}^{(0)}$ and $d_{\alpha,\beta}$, respectively, are nonzero for $\alpha, \beta = x, y$ only.

Under the combined action of nuclear field fluctuations, the electron-hole exchange interaction, and an external magnetic field, the exciton level splits into four sublevels ε_j ($j = 1$–4). Let us decompose the exciton eigenstates $\Psi^{(j)}$ into the basis states $\Psi_1, \Psi_x, \Psi_y, \Psi_4$:

$$\Psi^{(j)} = \sum_{m=1,x,y,4} C_m^{(j)} \Psi_m. \tag{9}$$

The coefficients $C_m^{(j)}$ form a unitary matrix and satisfy the identities

$$\sum_m C_m^{(j)} C_m^{(j')*} = \delta_{jj'}, \quad \sum_j C_m^{(j)} C_{m'}^{(j)*} = \delta_{mm'}. \tag{10}$$

We begin the description of polarized PL by considering the limit where the energy splittings between levels exceed by far their natural widths,

$$|E_j - E_{j'}| \gg \frac{\hbar}{\tau_j}, \frac{\hbar}{\tau_{j'}} \quad (j' \neq j), \tag{11}$$

with τ_j being the exciton lifetime in the state j. Then the interference of quantum states is negligible, and one can use the level populations f_j instead of the exciton spin-density matrix. In this case, the polarization matrix of the emitted light has the form

$$d_{\alpha\beta} = \sum_j d_{\alpha\beta}^{(j)} \propto M_0^2 \sum_j C_\alpha^{(j)*} C_\beta^{(j)} f_j, \qquad (12)$$

while the values of f_j are found from

$$\begin{aligned}
f_j &\propto \tau_j \left| C_x^{(j)*} e_x^{(0)} + C_y^{(j)*} e_y^{(0)} \right|^2 \\
&= \tau_j \Big[\left| C_x^{(j)} \right|^2 \left| e_x^{(0)} \right|^2 + \left| C_y^{(j)} \right|^2 \left| e_y^{(0)} \right|^2 \\
&\quad + 2\,\mathrm{Re}\big(C_x^{(j)*} C_y^{(j)} e_x^{(0)} e_y^{(0)*} \big) \Big].
\end{aligned} \qquad (13)$$

The polarization-independent prefactors are omitted in Eqs. (12) and (13). The inverse lifetimes of the excitonic sublevels contain two terms:

$$\frac{1}{\tau_j} = \frac{1}{\tau_r} \left(\left| C_x^{(j)} \right|^2 + \left| C_y^{(j)} \right|^2 \right) + \frac{1}{\tau_{\mathrm{nr}}}. \qquad (14)$$

They are determined by the radiative lifetime τ_r of the states (7) and the nonradiative lifetime τ_{nr}, which is independent of the index j.

The normalized Stokes parameters of the incident light are related with the polarization tensor $d_{\alpha\beta}^{(0)}$ by

$$P_l^{(0)} = \frac{d_{xx}^{(0)} - d_{yy}^{(0)}}{d_{xx}^{(0)} + d_{yy}^{(0)}}, \qquad P_{l'}^{(0)} = \frac{2\,\mathrm{Re}\{d_{xy}^{(0)}\}}{d_{xx}^{(0)} + d_{yy}^{(0)}},$$

$$P_c^{(0)} = -\frac{2\,\mathrm{Im}\{d_{xy}^{(0)}\}}{d_{xx}^{(0)} + d_{yy}^{(0)}}, \qquad (15)$$

where the components $d_{\alpha\beta}^{(0)}$ are proportional to the products $e_\alpha^{(0)} e_\beta^{(0)*}$ [44]. By analogy with Eq. (15), it is convenient to introduce the combinations

$$p_l^{(j)} = \frac{\left| C_x^{(j)} \right|^2 - \left| C_y^{(j)} \right|^2}{\left| C_x^{(j)} \right|^2 + \left| C_y^{(j)} \right|^2}, \qquad p_{l'}^{(j)} = \frac{2\,\mathrm{Re}\{C_x^{(j)} C_y^{(j)*}\}}{\left| C_x^{(j)} \right|^2 + \left| C_y^{(j)} \right|^2},$$

$$p_c^{(j)} = -\frac{2\,\mathrm{Im}\{C_x^{(j)} C_y^{(j)*}\}}{\left| C_x^{(j)} \right|^2 + \left| C_y^{(j)} \right|^2}. \qquad (16)$$

Expressing $C_\alpha^{(j)*} C_\beta^{(j)}$ and $e_\alpha^{(0)} e_\beta^{(0)*}$ in Eq. (13) through $p^{(j)}$ and $P_k^{(0)}$, we obtain

$$f_j \propto \tau_j \left(1 + \sum_{k=l,l',c} p_k^{(j)} P_k^{(0)} \right) \left(\left| C_x^{(j)} \right|^2 + \left| C_y^{(j)} \right|^2 \right). \qquad (17)$$

Note that here we omit the factor $d_{xx}^{(0)} + d_{yy}^{(0)}$, which is polarization independent and proportional to the initial light intensity.

Generally, the relation between the Stokes parameters of the secondary radiation P_k and the parameters $P_{k'}^{(0)}$ can be written as

$$P_k = \sum_{k'=l,l',c} \Lambda_{kk'} P_{k'}^{(0)}. \qquad (18)$$

Neglecting nonradiative recombination processes ($\tau_{\mathrm{nr}}/\tau_r \to \infty$), the PL intensity is independent of the polarization of the

exciting light, and the matrix $\hat{\Lambda}$ is given by

$$\Lambda_{kk'} = \frac{1}{2} \sum_{j=1}^{4} \left(\left| C_x^{(j)} \right|^2 + \left| C_y^{(j)} \right|^2 \right) p_k^{(j)} p_{k'}^{(j)}. \qquad (19)$$

For excitons with large exchange splitting between $\Psi_{1,4}$ and $\Psi_{x,y}$ pairs of states [see Eqs. (4) and (7)], the mixing between these pairs can be neglected, and it suffices for the calculation of the PL polarization to consider only the radiative doublet (7) [7,11]. In this limit, (i) the summation in Eq. (19) should be performed only over the two radiative states $j = 1, 2$, (ii) the sum $\left| C_x^{(j)} \right|^2 + \left| C_y^{(j)} \right|^2$ becomes equal to unity, and (iii) $p_k^{(1)} p_{k'}^{(1)} = p_k^{(2)} p_{k'}^{(2)}$.

III. NEGLECTING THE EXCHANGE INTERACTION AND NONRADIATIVE RECOMBINATION

In this section, we consider only the Zeeman interaction of an electron and a hole with an external magnetic field and the hyperfine interaction of an electron with the host lattice nuclei. Then the exciton Hamiltonian takes the form

$$\mathcal{H} = \frac{\hbar}{2} \big[(\boldsymbol{\Omega}_L^e + \boldsymbol{\Omega}_N) \cdot \boldsymbol{\sigma}_e + \boldsymbol{\Omega}_L^h \cdot \boldsymbol{\sigma}_h \big]. \qquad (20)$$

Here, $\boldsymbol{\sigma}_e$ and $\boldsymbol{\sigma}_h$ are the electron and hole vectors of Pauli matrices;

$$\boldsymbol{\Omega}_L^e = \frac{\mu_B}{\hbar} \hat{g}_e \boldsymbol{B}, \qquad \boldsymbol{\Omega}_L^h = \frac{\mu_B}{\hbar} \hat{g}_h \boldsymbol{B}$$

are the electron and hole spin precession frequencies in the magnetic field $\boldsymbol{B}$ with $\hat{g}_e$ and $\hat{g}_h$ being the tensors of the g factors; μ_B is the Bohr magneton; and $\boldsymbol{\Omega}_N$ is the electron spin precession frequency in the Overhauser field. The hole hyperfine interaction is suppressed because the hole Bloch functions $\mathcal{X}$ and $\mathcal{Y}$ vanish at the nuclear sites. So we neglect it, assuming that the corresponding hole spin precession frequency is smaller than the inverse exciton radiative lifetime. In practice, this assumption may be violated, which calls for a separate study. We also neglect phonon-assisted spin relaxation. The D_{2d} symmetry allows for the anisotropy of the hole g factor, which in the chosen basis has a simple form: $g_{h,zz} \equiv g_h^\parallel$, $g_{h,xx} = g_{h,yy} \equiv g_h^\perp$, and the other components are zero. Because of the weak spin-orbit coupling in X valleys, we neglect the anisotropy of the electron g factor and set $g_{e,\alpha\beta} = g_e \delta_{\alpha\beta}$ with $\alpha, \beta = x, y, z$, $\delta_{\alpha\beta}$ being the Kronecker delta and $g_e \approx 2$.

The nuclear spin dynamics typically takes place at the time scale of 0.1 ms [45]. This may be comparable to the lifetime of dark excitons in (In,Al)As/AlAs quantum dots [46], which may lead to peculiar features in the optical properties. However, we neglect the nuclear spin dynamics and assume $\boldsymbol{\Omega}_N$ to be "frozen" [38]. The electron intravalley hyperfine interaction can be anisotropic [47], but we neglect the anisotropy for simplicity as well as the intervalley hyperfine interaction [48]. As a result, the distribution function of the electron spin precession frequencies takes the form [45]

$$\mathcal{F}(\boldsymbol{\Omega}_N) = \left(\sqrt{\frac{2}{\pi}} T_2^* \right)^3 e^{-2(\Omega_N T_2^*)^2}, \qquad (21)$$

where the parameter T_2^* characterizes the dispersion

$$\langle \Omega_N^2 \rangle = \int \mathcal{F}(\boldsymbol{\Omega}_N) \boldsymbol{\Omega}_N^2 d\boldsymbol{\Omega}_N = \frac{3}{4} \frac{1}{T_2^{*2}}, \tag{22}$$

with $d\boldsymbol{\Omega}_N = d\Omega_{N,x} d\Omega_{N,y} d\Omega_{N,z}$. Additionally, the parameter T_2^* is a measure of the electron spin dephasing time.

According to the conditions (1), the electron spin precession with the frequency $\boldsymbol{\Omega}_N$ is faster than the exciton recombination rate [49,50]. For this reason, the direction of $\boldsymbol{\Omega}_e = \boldsymbol{\Omega}_L^e + \boldsymbol{\Omega}_N$ fixes the quantization axis for the electron spin, and the electron eigenstates are

$$\varphi_{\frac{1}{2}}^{(e)} = e^{-i\varphi/2} \cos\frac{\theta}{2} \psi_{\frac{1}{2}}^{(e)} + e^{i\varphi/2} \sin\frac{\theta}{2} \psi_{-\frac{1}{2}}^{(e)},$$

$$\varphi_{-\frac{1}{2}}^{(e)} = -e^{-i\varphi/2} \sin\frac{\theta}{2} \psi_{\frac{1}{2}}^{(e)} + e^{i\varphi/2} \cos\frac{\theta}{2} \psi_{-\frac{1}{2}}^{(e)}, \tag{23}$$

where θ and φ are the polar and azimuthal angles of $\boldsymbol{\Omega}_e$. It is convenient to use the exciton spin-density matrix $\hat{\rho}$ in the basis $\Phi_{jm} = \varphi_j^{(e)} \psi_m^{(h)}$ ($j, m = \pm 1/2$), instead of the basis (4).

For zero exchange interaction, the matrix $\hat{\rho}$ is block diagonal in the electron spin subspace:

$$\rho_{j'm', jm} = \delta_{j'j} \rho_{m',m}^{(j)}. \tag{24}$$

The hole 2×2 spin-density matrix can be conveniently presented in the form

$$\hat{\rho}^{(j)} = \begin{bmatrix} \frac{N^{(j)}}{2} + J_z^{(j)} & J_x^{(j)} - iJ_y^{(j)} \\ J_x^{(j)} + iJ_y^{(j)} & \frac{N^{(j)}}{2} - J_z^{(j)} \end{bmatrix}, \tag{25}$$

where $N^{(j)}$ is the number of excitons with the electron spin $j = \pm 1/2$ and $\boldsymbol{J}^{(j)}$ is the quantum statistical average of the hole spin for the corresponding value of j and can take arbitrary values between $-1/2$ and $1/2$.

We consider resonant exciton excitation with the rate G and take into account a single decay channel in the system, namely, the radiative exciton recombination with the time τ_r defined in Eq. (14). In contrast to the previous section, the product $\Omega_L^h \tau_r$ can be arbitrary. The kinetic equations for $N^{(1/2)}$ and $\boldsymbol{J}^{(1/2)}$ take the form

$$\frac{dN^{(\frac{1}{2})}}{dt} = G\frac{1 - P_c^{(0)}\cos\theta}{2} - \frac{1}{\tau_r}\left(\frac{N^{(\frac{1}{2})}}{2} + J_z^{(\frac{1}{2})}\cos\theta\right), \tag{26a}$$

$$\frac{dJ_z^{(\frac{1}{2})}}{dt} = \Omega_{L,x}^h J_y^{(\frac{1}{2})} - \Omega_{L,y}^h J_x^{(\frac{1}{2})} + \frac{G}{4}\left(-P_c^{(0)} + \cos\theta\right) - \frac{1}{\tau_r}\left(\frac{J_z^{(\frac{1}{2})}}{2} + \frac{N^{(\frac{1}{2})}}{4}\cos\theta\right), \tag{26b}$$

$$\frac{dJ_x^{(\frac{1}{2})}}{dt} = \Omega_{L,y}^h J_z^{(\frac{1}{2})} - \Omega_{L,z}^h J_y^{(\frac{1}{2})} + \frac{G}{4}\sin\theta\left(P_l^{(0)}\cos\varphi - P_{l'}^{(0)}\sin\varphi\right) - \frac{J_x^{(\frac{1}{2})}}{2\tau_r}, \tag{26c}$$

$$\frac{dJ_y^{(\frac{1}{2})}}{dt} = \Omega_{L,z}^h J_x^{(\frac{1}{2})} - \Omega_{L,x}^h J_z^{(\frac{1}{2})} - \frac{G}{4}\sin\theta\left(P_l^{(0)}\sin\varphi + P_{l'}^{(0)}\cos\varphi\right) - \frac{J_y^{(\frac{1}{2})}}{2\tau_r}, \tag{26d}$$

with $P_k^{(0)}$ ($k = l, l', c$) being the Stokes parameters of the incident light, Eq. (15). The generation terms proportional to G are derived taking into account that the wave function excited by the coherent light has the form $\Psi^{(0)} = e_x^{(0)}\Psi_x + e_y^{(0)}\Psi_y$. Under the continuous excitation, the time derivatives in Eq. (26) vanish, and the steady state is established, which allows one to solve the equations and find the time-independent variables $N^{(1/2)}$ and $J_\alpha^{(1/2)}$.

The intensities of circularly and linearly polarized PL in the z direction read

$$I_+^{(\frac{1}{2})} = \frac{N^{(\frac{1}{2})} - 2J_z^{(\frac{1}{2})}}{2\tau_r}(1 - \cos\theta), \quad I_-^{(\frac{1}{2})} = \frac{N^{(\frac{1}{2})} + 2J_z^{(\frac{1}{2})}}{2\tau_r}(1 + \cos\theta), \tag{27a}$$

$$I_x^{(\frac{1}{2})} = \frac{1}{\tau_r}\left[\frac{N^{(\frac{1}{2})}}{2} + J_z^{(\frac{1}{2})}\cos\theta + \sin\theta\left(J_x^{(\frac{1}{2})}\cos\varphi - J_y^{(\frac{1}{2})}\sin\varphi\right)\right], \tag{27b}$$

$$I_y^{(\frac{1}{2})} = \frac{1}{\tau_r}\left[\frac{N^{(\frac{1}{2})}}{2} + J_z^{(\frac{1}{2})}\cos\theta - \sin\theta\left(J_x^{(\frac{1}{2})}\cos\varphi - J_y^{(\frac{1}{2})}\sin\varphi\right)\right],$$

$$I_{x'}^{(\frac{1}{2})} = \frac{1}{\tau_r}\left[\frac{N^{(\frac{1}{2})}}{2} + J_z^{(\frac{1}{2})}\cos\theta - \sin\theta\left(J_x^{(\frac{1}{2})}\sin\varphi + J_y^{(\frac{1}{2})}\cos\varphi\right)\right],$$

$$I_{y'}^{(\frac{1}{2})} = \frac{1}{\tau_r}\left[\frac{N^{(\frac{1}{2})}}{2} + J_z^{(\frac{1}{2})}\cos\theta + \sin\theta\left(J_x^{(\frac{1}{2})}\sin\varphi + J_y^{(\frac{1}{2})}\cos\varphi\right)\right]. \tag{27c}$$

Equations for $N^{(-1/2)}$, $\boldsymbol{J}^{(-1/2)}$ and the corresponding intensities have the same form as Eqs. (26) and (27), but with the replacement of $\cos\theta$ and $\sin\theta$ with $-\cos\theta$ and $-\sin\theta$.

A. Longitudinal magnetic field (Faraday geometry)

In the longitudinal magnetic field, the substitution of the solution of Eq. (26) into Eq. (27) yields

$$\hat{\Lambda} = \begin{pmatrix} \frac{\sin^2\theta}{1+(2\Omega^h_{L,z}\tau_r)^2} & \frac{2\Omega^h_{L,z}\tau_r\sin^2\theta}{1+(2\Omega^h_{L,z}\tau_r)^2} & 0 \\ -\frac{2\Omega^h_{L,z}\tau_r\sin^2\theta}{1+(2\Omega^h_{L,z}\tau_r)^2} & \frac{\sin^2\theta}{1+(2\Omega^h_{L,z}\tau_r)^2} & 0 \\ 0 & 0 & 1 \end{pmatrix}. \tag{28}$$

The multiplier 2 before $\Omega^h_{L,z}\tau_r$ reflects the fact that for the fast hole spin precession the bright excitons are equally mixed with the dark ones. This expression should be averaged over the random Overhauser fields as follows:

$$\langle\hat{\Lambda}\rangle = \int \hat{\Lambda}\mathcal{F}(\boldsymbol{\Omega}_N)d\boldsymbol{\Omega}_N. \tag{29}$$

The integration can be readily performed using the equation [51,52]

$$\langle\sin^2\theta\rangle = \frac{1}{2(\Omega^e_L T^*_2)^2}\left[1 - \frac{1}{\sqrt{2}\Omega^e_L T^*_2}D(\sqrt{2}\Omega^e_L T^*_2)\right]$$
$$\approx \frac{2}{3}\frac{1}{1+(\Omega^e_L T^*_2)^2}, \tag{30}$$

where $D(x) = \exp(-x^2)\int_0^x \exp(y^2)dy$ is the Dawson integral. The approximation reproduces the exact function up to 4%.

In the realistic case of $\Omega^e_L T^*_2 \ll \Omega^h_L\tau_r$ or $g_e T^*_2 \ll g^{\parallel}_h\tau_r$ (we remind the reader that $1/\Omega_N \sim T^*_2 \ll \tau_r$), we obtain from Eqs. (28)–(30)

$$\langle\hat{\Lambda}\rangle = \begin{pmatrix} \frac{2/3}{1+(2\Omega^h_{L,z}\tau_r)^2} & \frac{(4/3)\Omega^h_{L,z}\tau_r}{1+(2\Omega^h_{L,z}\tau_r)^2} & 0 \\ -\frac{(4/3)\Omega^h_{L,z}\tau_r}{1+(2\Omega^h_{L,z}\tau_r)^2} & \frac{2/3}{1+(2\Omega^h_{L,z}\tau_r)^2} & 0 \\ 0 & 0 & 1 \end{pmatrix}. \tag{31}$$

The two different nontrivial components of this matrix are shown in Fig. 1(a). This nonstandard formalism was introduced in Ref. [32], and it is illustrated in the inset in Fig. 1(a). In the illustration we show the case of electron spin parallel to $\boldsymbol{\Omega}^e_L$, so it makes an angle θ with the z axis. The electron spin is fixed, and the exciton spin dynamics is governed by the precession of the hole spin $\boldsymbol{J}^{(1/2)}$ (in the subspace of the given electron spin direction) with the frequency $\boldsymbol{\Omega}^h_L$. In addition, one has to consider separately the dynamics of $\boldsymbol{J}^{(-1/2)}$ for the electron spin antiparallel to $\boldsymbol{\Omega}^e_L$.

B. Transverse magnetic field (Voigt geometry)

In the transverse magnetic field, the nonzero components of the hole spin precession frequency $\boldsymbol{\Omega}^h_L$ are $\Omega^h_{L,x} = \Omega^h_L\cos\alpha$ and $\Omega^h_{L,y} = \Omega^h_L\sin\alpha$, where α is the angle between $\boldsymbol{\Omega}^h_L$ and the x axis. Then we obtain from Eqs. (26) and (27)

$$\hat{\Lambda} = \begin{pmatrix} \sin^2\theta\cos^2(\varphi+\alpha) & -\frac{1}{2}\sin^2\theta\sin(2\varphi+2\alpha) & 0 \\ -\frac{1}{2}\sin^2\theta\sin(2\varphi+2\alpha) & \sin^2\theta\sin^2(\varphi+\alpha) & 0 \\ 0 & 0 & \cos^2\theta \end{pmatrix}$$
$$+ \frac{\sin^4\theta}{\sin^2\theta+(2\Omega^h_L\tau_r)^2}\begin{pmatrix} \sin^2(\varphi+\alpha) & \frac{1}{2}\sin(2\varphi+2\alpha) & 0 \\ \frac{1}{2}\sin(2\varphi+2\alpha) & \cos^2(\varphi+\alpha) & 0 \\ 0 & 0 & 1 \end{pmatrix}. \tag{32}$$

Averaging the matrix $\hat{\Lambda}$ in the same way as in Sec. III A, we obtain

$$\langle\hat{\Lambda}\rangle = \frac{1}{(\Omega^e_L T^*_2)^2+1}\begin{pmatrix} \frac{1}{3}+\cos^2(2\alpha)(\Omega^e_L T^*_2)^2 & -\frac{1}{2}\sin(4\alpha)(\Omega^e_L T^*_2)^2 & 0 \\ -\frac{1}{2}\sin(4\alpha)(\Omega^e_L T^*_2)^2 & \frac{1}{3}+\sin^2(2\alpha)(\Omega^e_L T^*_2)^2 & 0 \\ 0 & 0 & \frac{1}{3} \end{pmatrix} + \frac{1/3}{1+5(\Omega^h_L\tau_r)^2}\begin{pmatrix} 1 & 0 & 0 \\ 0 & 1 & 0 \\ 0 & 0 & 2 \end{pmatrix}.$$

Notably, this expression reveals an anisotropy of the quantum dot having the D_{2d} symmetry. This anisotropy originates from the fixed orbitals $\mathcal{X}, \mathcal{Y}$ in the basis (3) which defines the selection rules for linearly polarized light and the heavy-hole Zeeman Hamiltonian (20) [53]. As a result, the polarization of the emitted light depends not only on the angle between polarization of the exciting light and magnetic field, but also on their orientation with respect to the crystallographic axes.

In the limit of strong magnetic field, $\Omega^e_L T^*_2 \gg 1$, we obtain

$$\langle\hat{\Lambda}\rangle = \begin{pmatrix} \cos^2(2\alpha) & -\frac{1}{2}\sin(4\alpha) & 0 \\ -\frac{1}{2}\sin(4\alpha) & \sin^2(2\alpha) & 0 \\ 0 & 0 & 0 \end{pmatrix}. \tag{33}$$

First, we note that this expression can be obtained from Eq. (32) using $\theta = \pi/2$ and $\phi = \alpha$. Second, it can be obtained from Eq. (19) from the previous section using the eigenfunctions

$$\Psi^{(1)} = (\Psi_2 + e^{i\alpha}\Psi_1 + e^{i\alpha}\Psi_4 + e^{2i\alpha}\Psi_3)/2, \tag{34a}$$

$$\Psi^{(2)} = (\Psi_2 - e^{i\alpha}\Psi_1 + e^{i\alpha}\Psi_4 - e^{2i\alpha}\Psi_3)/2, \tag{34b}$$

$$\Psi^{(3)} = (\Psi_2 + e^{i\alpha}\Psi_1 - e^{i\alpha}\Psi_4 - e^{2i\alpha}\Psi_3)/2, \tag{34c}$$

$$\Psi^{(4)} = (\Psi_2 - e^{i\alpha}\Psi_1 - e^{i\alpha}\Psi_4 + e^{2i\alpha}\Psi_3)/2, \tag{34d}$$

which give the coefficients $|C^{(j)}_x|^2 + |C^{(j)}_y|^2 = 1/2$ for all j and polarizations $p^{(1)}_l = p^{(4)}_l = -p^{(2)}_l = -p^{(3)}_l = \cos(2\alpha)$, $p^{(2)}_{l'} = p^{(3)}_{l'} = -p^{(1)}_{l'} = -p^{(4)}_{l'} = \sin(2\alpha)$, and $p^{(j)}_c = 0$ for all j.
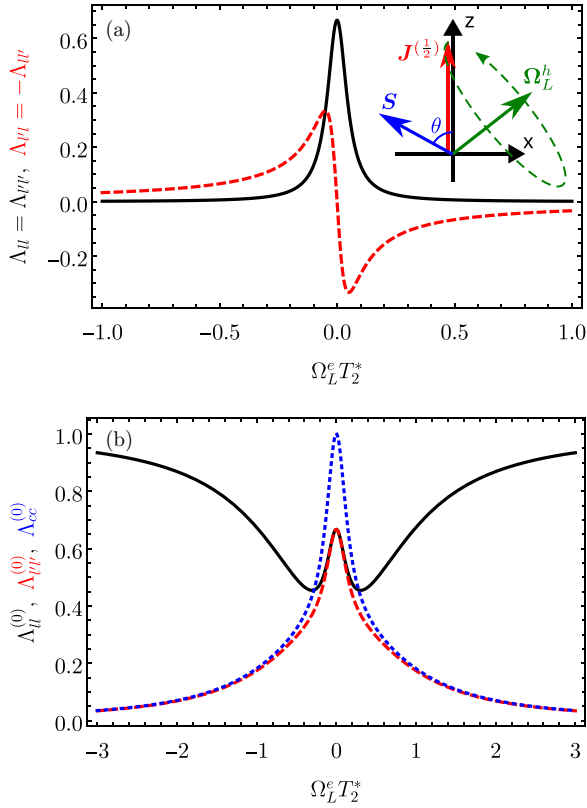
FIG. 1. (a) Coefficients $\Lambda_{ll} = \Lambda_{l'l'}$ (black solid curve) and $\Lambda_{l'l} = -\Lambda_{ll'}$ (red dashed curve), calculated after Eq. (31) as the functions of the longitudinal magnetic field for $g_h^\parallel \tau_r = 10 g_e T_2^*$. The inset illustrates the fixed electron spin ($\boldsymbol{S}$) directed along $\boldsymbol{\Omega}_L^e$, which makes an angle θ with the z axis, and the precession of the corresponding hole spin $\boldsymbol{J}^{(1/2)}$ with the frequency $\boldsymbol{\Omega}_L^h$. (b) Diagonal components of the matrix $\hat{\Lambda}^{(0)}$ calculated after Eq. (35) as functions of the transverse magnetic field for $g_h^\perp \tau_r = 3 g_e T_2^*$. The exciton optical alignment along and across the magnetic field, $\Lambda_{ll}^{(0)}$, is shown by the black solid curve; the alignment in the axes rotated by $\pi/4$, $\Lambda_{l'l'}^{(0)}$, is shown by the red dashed curve, and the optical orientation, $\Lambda_{cc}^{(0)}$ is shown by the blue dotted curve.

In the following, we focus on the specific case of $\alpha = 0$. Denoting the matrix $\hat{\Lambda}$ at $\alpha = 0$ as $\hat{\Lambda}^{(0)}$, we have

$$
\langle \hat{\Lambda}^{(0)} \rangle = \begin{pmatrix} \frac{(\Omega_L^e T_2^*)^2 + 1/3}{(\Omega_L^e T_2^*)^2 + 1} & 0 & 0 \\ 0 & \frac{1/3}{(\Omega_L^e T_2^*)^2 + 1} & 0 \\ 0 & 0 & \frac{1/3}{(\Omega_L^e T_2^*)^2 + 1} \end{pmatrix}
$$

$$
+ \frac{1/3}{1 + 5(\Omega_L^h \tau_r)^2} \begin{pmatrix} 1 & 0 & 0 \\ 0 & 1 & 0 \\ 0 & 0 & 2 \end{pmatrix}. \tag{35}
$$

In this case, there is no polarization conversion. The three diagonal components of the matrix $\hat{\Lambda}^{(0)}$ are shown in Fig. 1(b) as functions of the magnetic field. Notably for α being a multiple of $\pi/4$, the matrix $\langle \hat{\Lambda} \rangle$ has the same form in the rotated coordinate frame x', y', z with the x' axis parallel to the direction of the magnetic field.
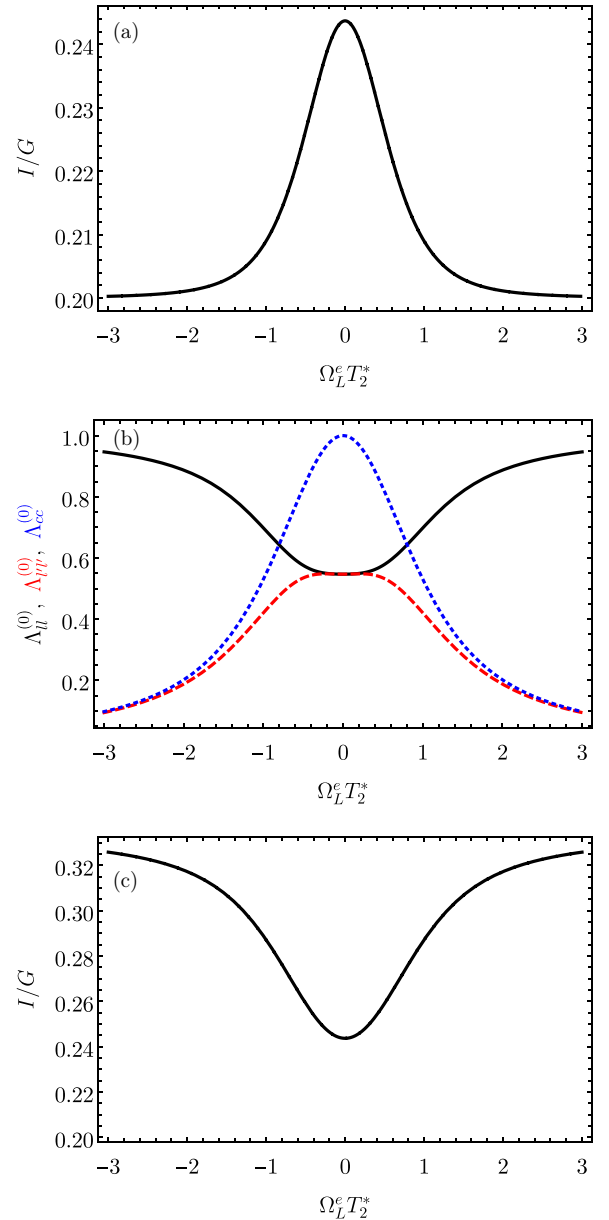

FIG. 2. The PL intensity (a) and polarization (b) as a function of the transverse magnetic field $\boldsymbol{B} \parallel x$. The solid, dashed, and dotted curves are the degrees of polarization P_l, $P_{l'}$, and P_c under excitation by light of the corresponding polarization $P_l^{(0)} = 1$, $P_{l'}^{(0)} = 1$, and $P_c^{(0)} = 1$. (c) Magnetic field dependence of the PL intensity at $\boldsymbol{B} \parallel z$.

IV. ROLE OF NONRADIATIVE RECOMBINATION

Let us take into account the nonradiative recombination time τ_{nr} satisfying the condition (1). Then one should replace d/dt with $d/dt + 1/\tau_{nr}$ in the kinetics equations (26). At the same time, in the expressions for the PL intensities (27), the common factor τ_r^{-1} remains unchanged. As a consequence, the PL intensity becomes dependent on the magnetic field, and this is the most important manifestation of the nonradiative recombination channel.

Figure 2 shows the PL intensity and polarization as functions of the transverse (a, b) and longitudinal (c) magnetic field calculated for $\tau_{nr} = \tau_r/2$ and the same other parameters

as in Fig. 1. In the absence of magnetic field, the total PL intensity

$$I = I_+^{(1/2)} + I_-^{(1/2)} + I_+^{(-1/2)} + I_-^{(-1/2)}$$

is given by

$$I = G \left[1 - 2 \frac{\tau_r}{\tau_{\mathrm{nr}}} + 2 \frac{\tau_r^2}{\tau_{\mathrm{nr}}^2} \ln \left(\frac{\tau_r + \tau_{\mathrm{nr}}}{\tau_r} \right) \right]. \tag{36}$$

In a longitudinal magnetic field B_z, due to the time-reversal symmetry, the intensity I is an even function of B_z. Therefore this function is an invariant of the symmetry group D_{2d} (representation Γ_1) and does not depend on the excitation polarization since the differences $I_x - I_y$, $I_{x'} - I_{y'}$, and $I_+ - I_-$, I_k being $I_k^{(1/2)} + I_k^{(-1/2)}$, belong to the representations Γ_3, Γ_4, $\Gamma_2 \neq \Gamma_1$, respectively. As a result, the curve in Fig. 2(c) does not depend on the excitation polarization. It shows an increase in the PL intensity up to

$$I = \frac{G \tau_{\mathrm{nr}}}{\tau_r + \tau_{\mathrm{nr}}} \tag{37}$$

with the increasing longitudinal magnetic field.

In a transverse field, the dependence $I(B_x)$ is also even in B_x. It is convenient to present the square B_x^2 as the invariant $(B_x^2 + B_y^2)/2$ and the difference $(B_x^2 - B_y^2)/2$ that transforms according to the representation Γ_3. It follows then that the intensity I is insensitive to the Stokes parameters $P_{l'}^{(0)}$ and $P_c^{(0)}$ but can depend on P_l. The calculation, however, shows that under the condition $|g_h^\perp / g_e| \ll 1$ the dependence of I on $P_l^{(0)}$ vanishes, and the dependence of $I(B_x)$ is the same for all excitation polarizations [Fig. 2(a)]. In a strong transverse magnetic field, the intensity decreases to

$$I = \frac{G \tau_{\mathrm{nr}}}{2 \tau_r + \tau_{\mathrm{nr}}}. \tag{38}$$

The magnetic field dependences of polarizations vary continuously with the decreasing time τ_{nr}. The remarkable peak-to-valley ratio of the $P_l(B_z)$ curve in Fig. 1(b) decreases with the increasing role of the nonradiative recombination, and for $\tau_{\mathrm{nr}} = 0.5 \tau_r$ the peak disappears.

V. ROLE OF EXCHANGE INTERACTION

The short-range exchange interaction between an electron and a hole is described by the Hamiltonian [10]

$$V_{\mathrm{exch}} = \hbar \delta_0 \sigma_{e,z} \sigma_{h,z} / 2, \tag{39}$$

where δ_0 is the splitting between dark and bright excitonic states, which acts as a perturbation [7]. The long-range exchange interaction is strongly suppressed for momentum-indirect excitons [54]. Figure 3 shows the modification of the PL intensity dependence on the transverse magnetic field by the exchange interaction. It is calculated numerically using the spin-density matrix formalism with the same parameters as for Fig. 2(a) and $T_2^*/\tau_r = 0.005$. The total intensity weakly depends on the polarization of the excitation, and so we show the results for the unpolarized excitation to be specific. One can see that increase of the exchange interaction leads to the disappearance of this dependence due to the weakened mixing between bright and dark excitons. This takes place at
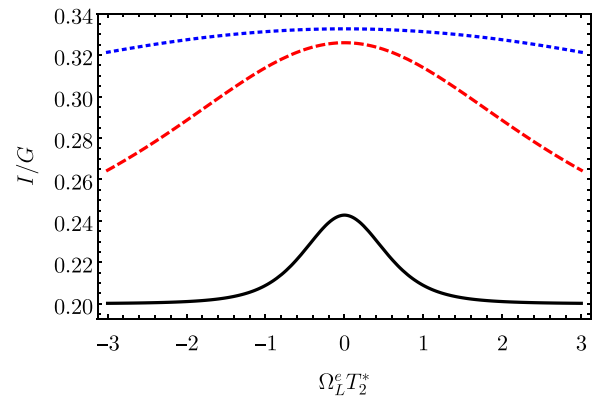

FIG. 3. Dependence of the PL intensity on the magnetic field applied in the Voigt geometry for the different exchange interaction strengths $\delta_0 T_2^* = 0$ (black solid curve), 3 (red dashed curve), and 10 (blue dotted curve).

$\delta_0 \sim 1/T_2^*$, and in the limit of $\delta_0 T_2^* \gg 1$ the intensity saturates at the value given by Eq. (37) similarly to the strong longitudinal magnetic field.

However, a much weaker exchange interaction $\delta_0 \sim 1/\tau_r$ can strongly modify the polarization of the PL. This effect can be described by Eqs. (26) and (27) with the only replacement $\Omega_{L,z}^h \rightarrow \Omega_{L,z}^h + \delta_0 \cos \theta$, which can be seen from Eq. (39). The result of the calculation is shown in Fig. 4 for the same parameters as in Fig. 1 (without nonradiative recombination) and different strengths of the exchange interaction. One can see that the increase of the exchange interaction reverses the narrow component of $\Lambda_{ll}^{(0)}(B_x)$: A dip in the polarization becomes deeper. This effect can be described analytically similarly to Sec. III, but the result turns out to be too cumbersome.

VI. DISCUSSION AND CONCLUSION

Figures 1–4 illustrate the characteristics of resonant polarized PL spectroscopy of d-r–ind-k quantum dots. Due to
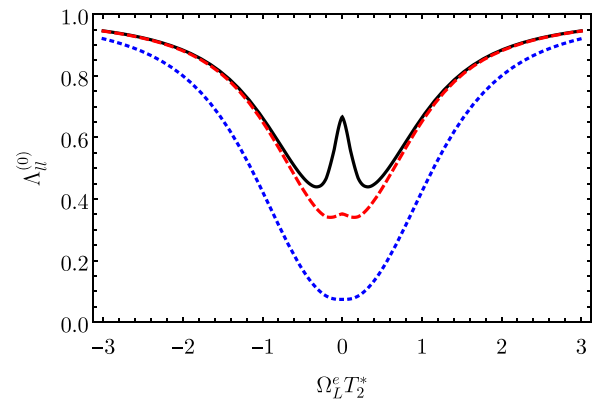

FIG. 4. Dependence of the PL linear polarization degree $\Lambda_{ll}^{(0)}$ on the magnetic field applied in the Voigt geometry for the different exchange interaction strengths $\delta_0 \tau_r = 0$ (black solid curve), 1.5 (red dashed curve), and 10 (blue dotted curve). Note the difference in the scale of the exchange interaction compared with Fig. 3. The alignment monotonously decreases with increase of δ_0.

small exchange splitting in these dots, the fluctuations of the Overhauser field have a significant effect on the electron spin. As a consequence, at zero magnetic field in the absence of exchange interaction and spin-lattice relaxation, the degree of PL linear polarization excited by linearly polarized light decreases to 2/3; see Eqs. (31) and (33) for $\langle \hat{\Lambda} \rangle$. Inclusion of a weak short-range exchange interaction (39) results in an additional reduction of the exciton alignment, which has a double-scale character. At the scale $\delta_0 \sim 1/\tau_r \ll 1/T_N^*$, the electron spin states (23) are unaffected by the exchange interaction, but the electron occupying these states partially depolarizes the hole spin. As δ_0 increases to $10\tau_r^{-1}$, the linear polarization at zero magnetic field decreases from 2/3 to 0.1.

If δ_0 prevails over the nuclear fluctuations $\sqrt{\langle \Omega_N^2 \rangle} \propto 1/T_2^*$, the exchange interaction suppresses the influence of the lateral component $\boldsymbol{\Omega}_N$ of the nuclear field, thereby increasing the effect of the longitudinal component $\Omega_{N,z}$ on the electron. Note that, in d-r–d-k quantum wells, the radiative damping τ_r^{-1} exceeds Ω_N by far, the nuclear field has no time to produce a depolarizing influence, and the degree of linear polarization P_l or $P_{l'}$ may reach 100%.

Application of the longitudinal magnetic field results in a hole spin precession which, in its turn, leads to the conversion of linear polarizations $P_l \leftrightarrow P_{l'}$ and an overall decrease of optical alignment [dashed and solid curves in Fig. 1(a)], similarly to the polarization behavior in conventional d-r–d-k quantum dots.

An external transverse magnetic field leads to the mixing of hole spin-up and spin-down states controlled by the transverse g factor $g_h^\perp$. This results in a partial suppression of the optical orientation. When the magnetic field reaches the value of typical Overhauser field fluctuations, the electron spin states also get affected. With further increase of the field, the optical orientation vanishes, as shown in Fig. 1(b). The field-induced mixing of the spin states also suppresses the optical alignment component $\Lambda_{l'l'}^{(0)}$.

The alignment component $\Lambda_{ll}^{(0)}$ shows quite different behavior [black solid curve in Fig. 1(b)]. At $\Omega_L^e T_2^* < 1$, the electron spin states (23) are unaffected by the magnetic field while the hole spin states are depolarized at $\Omega_L^h \tau_r \gtrsim 1$, and the polarization P_l decreases with the increasing field. However, the strong magnetic field, $\Omega_L^e T_2^* \gg 1$, suppresses the nuclear field and tends to form both the electron and hole eigenstates with the spins parallel or antiparallel to $\boldsymbol{B}$. As a result, in the geometry $\boldsymbol{B} \parallel x$ among four exciton split sublevels (34), two are active in the x polarization, the remaining two are y polarized, and one has $P_l = P_l^{(0)}$.

The nonradiative exciton recombination manifests itself by expected dependence of the PL intensity on the transverse magnetic field [Fig. 2(a)]. The larger the magnetic field, the stronger the mixing between bright and dark states, and the smaller the intensity. The longitudinal magnetic field acts in the opposite way: It cancels out the effect of the nuclear field and decouples the bright and dark excitons causing growth of the PL intensity, as shown in Fig. 2(c). Qualitatively, the dependences of P_l, $P_{l'}$, and P_c on the transverse magnetic

field remain the same as in Fig. 1(b) obtained in the absence of nonradiative recombination, but they get smoother. In particular, the peak with two symmetrical valleys in the component $\Lambda_{ll}^{(0)}$ disappears. This happens because the width of this peak is determined by the exciton lifetime, and the nonradiative recombination reduces this time, thus broadening the peak, which leads to its disappearance for the chosen parameters.

The strong exchange splitting, $\delta_0 \gtrsim 1/T_2^*$, suppresses mixing between the bright and dark exciton states. As a result, the effect of the transverse magnetic field on the PL intensity is reduced, and the dependence $I(B)$ becomes weaker and broader, as one can see in Fig. 3.

As mentioned above, the magnetic dipole-dipole hole-nuclear interaction can play a role if the corresponding hole spin precession frequency Ω_N^h is larger than the exciton inverse lifetime. An analysis of the model where Ω_N^h is nonzero will be reported elsewhere. Also, it would be interesting to generalize the developed theory for quantum dots of the C_{2v} symmetry, where the two different contributions to the transverse hole g factor are symmetry allowed. The role of intervalley scattering in (In,Al)As/AlAs quantum dots is not clear yet. For moiré excitons in bilayers of transition metal dichalcogenides the ground electron and hole states form a quadruplet of excitons with selection rules like those in Eq. (6). With this in mind, we can predict similar physics except for the much smaller transverse electron and hole g factors, which describe intervalley mixing.

In conclusion, we have developed a theory of polarized PL of excitons confined in quantum dot structures with weak electron-hole exchange interaction. The particular nanosystem can be realized in quantum dots where the excitons are indirect either in the real or reciprocal space. For them the leading role is played by the electron-nuclear hyperfine interaction. We have derived a relation between the PL Stokes parameters and those of the exciting light, which can be directly observed in future experiments. It is quite different from the similar relation for conventional nano-objects with excitons characterized by a strong exchange interaction and short lifetimes. In particular, the optical alignment can be a nonmonotonic function of the transverse magnetic field. We have started with the model of vanishing exchange interaction and nonradiative exciton recombination and then took them into consideration. The present work opens up exciting possibilities in exciton physics and can be applied to study the confined excitons in (In,Al)As/AlAs quantum dots, interlayer excitons in transition metal dichalcogenides, etc.

[1] A. I. Ekimov and A. A. Onushchenko, Quantum size effect in three-dimensional microscopic semiconductor crystals, Pis'ma Zh. Eksp. Teor. Phys. **34**, 363 (1981) [JETP Lett. **34**, 345 (1981)].

[2] R. Rossetti, S. Nakahara, and L. E. Brus, Quantum size effects in the redox potentials, resonance Raman spectra, and electronic spectra of CdS crystallites in aqueous solution, J. Chem. Phys. **79**, 1086 (1983).

[3] L. Goldstein, F. Glas, J. Y. Marzin, M. N. Charasse, and G. Le Roux, Growth by molecular beam epitaxy and characterization of InAs/GaAs strained-layer superlattices, Appl. Phys. Lett. **47**, 1099 (1985).

[4] Zh. I. Alferov, The history and future of semiconductor heterostructures from the point of view of a Russian scientist, Phys. Scr. **T68**, 32 (1996).

[5] C. B. Murray, C. R. Kagan, and M. G. Bawendi, Synthesis and characterization of monodisperse nanocrystals and close-packed nanocrystal assemblies, Annu. Rev. Mater. Sci. **30**, 545 (2000).

[6] K. P. Sathe, N. S. Garud, V. B. Bangar, and N. R. Gadakh, A review on quantum dots (QDs), J. Adv. Sci. Res. **13**, 23 (2022).

[7] E. L. Ivchenko, *Optical Spectroscopy of Semiconductor Nanostructures* (Alpha Science International, Harrow, UK, 2005).

[8] M. Grundmann, *The Physics of Semiconductors: An Introduction Including Nanophysics and Applications*, 2nd ed. (Springer-Verlag, Berlin, 2010).

[9] E. L. Ivchenko, Spectroscopy of spin-polarized excitons in semiconductors, Pure Appl. Chem. **67**, 463 (1995).

[10] E. L. Ivchenko, Fine structure of excitonic levels in semiconductor nanostructures, Phys. Status Solidi A **164**, 487 (1997).

[11] R. I. Dzhioev, B. P. Zakharchenya, E. L. Ivchenko, V. L. Korenev, Yu. G. Kusrayev, N. N. Ledentsov, V. M. Ustinov, A. E. Zhukov, and A. F. Tsatsul'nikov, Optical orientation and alignment of excitons in quantum dots, Fiz. Tverd. Tela **40**, 858 (1998) [Phys. Solid State **40**, 790 (1998)].

[12] M. Paillard, X. Marie, P. Renucci, T. Amand, A. Jbeli, and J. M. Gérard, Spin relaxation quenching in semiconductor quantum dots, Phys. Rev. Lett. **86**, 1634 (2001).

[13] Yu. G. Kusrayev, A. V. Koudinov, B. P. Zakharchenya, S. Lee, J. K. Furdyna, and M. Dobrowolska, Optical orientation and alignment of excitons in self-assembled CdSe/ZnSe quantum dots: The role of excited states, Phys. Rev. B **72**, 155301 (2005).

[14] D. Lagarde, A. Balocchi, H. Carrère, P. Renucci, T. Amand, X. Marie, S. Founta, and H. Mariette, Room-temperature optical orientation of the exciton spin in cubic GaN/AlN quantum dots, Phys. Rev. B **77**, 041304(R) (2008).

[15] T. Belhadj, C.-M. Simon, T. Amand, P. Renucci, B. Chatel, O. Krebs, A. Lemaitre, P. Voisin, X. Marie, and B. Urbaszek, Controlling the polarization eigenstate of a quantum dot exciton with light, Phys. Rev. Lett. **103**, 086601 (2009).

[16] F. Hatami, N. N. Ledentsov, M. Grundmann, J. Böhrer, F. Heinrichsdorff, M. Beer, D. Bimberg, S. S. Ruvimov, P. Werner, U. Gösele, J. Heydenreich, U. Richter, S. V. Ivanov, B. Ya. Meltser, P. S. Kop'ev, and Zh. I. Alferov, Radiative recombination in type-II GaSb/GaAs quantum dots, Appl. Phys. Lett. **67**, 656 (1995).

[17] S. Kim, B. Fisher, H.-J. Eisler, and M. Bawendi, Type-II quantum dots: CdTe/CdSe (Core/Shell) and CdSe/ZnTe (Core/Shell) heterostructures, J. Am. Chem. Soc. **125**, 11466 (2003).

[18] R. Pandya, V. Steinmetz, Y. Puttisong, M. Dufour, Weimin M. Chen, R. Y. S. Chen, T. Barisien, A. Sharma, G. Lakhwani, A. Mitioglu, P. C. M. Christianen, L. Legrand, F. Bernardot, C. Testelin, A. W. Chin, S. Ithurria, M. Chamarro, and A. Rao, Fine structure and spin dynamics of linearly polarized indirect excitons in two-dimensional CdSe/CdTe colloidal heterostructures, ACS Nano **13**, 10140 (2019).

[19] P. Rivera, H. Yu, K. L. Seyler, N. P. Wilson, W. Yao, and X. Xu, Interlayer valley excitons in heterobilayers of transition metal dichalcogenides, Nat. Nanotechnol. **13**, 1004 (2018).

[20] E. M. Alexeev, N. Mullin, P. Ares, H. Nevison-Andrews, O. Skrypka, T. Godde, A. Kozikov, L. Hague, Y. Wang, K. S. Novoselov, L. Fumagalli, J. K. Hobbs, and A. I. Tartakovskii, Emergence of highly linearly polarized interlayer exciton emission in MoSe$_2$/WSe$_2$ heterobilayers with transfer-induced layer corrugation, ACS Nano **14**, 11110 (2020).

[21] Y. Bai, L. Zhou, J. Wang, W. Wu, L. J. McGilly, D. Halbertal, C. F. B. Lo, F. Liu, J. Ardelean, P. Rivera, N. R. Finney, X.-C. Yang, D. N. Basov, W. Yao, X. Xu, J. Hone, A. N. Pasupathy, and X.-Y. Zhu, Excitons in strain-induced one-dimensional moiré potentials at transition metal dichalcogenide heterojunctions, Nat. Mater. **19**, 1068 (2020).

[22] D. S. Smirnov, Dynamic valley polarization in moiré quantum dots, Phys. Rev. B **104**, L241401 (2021).

[23] V. V. Belykh, M. L. Skorikov, E. V. Kulebyakina, E. V. Kolobkova, M. S. Kuznetsova, M. M. Glazov, and D. R. Yakovlev, Submillisecond spin relaxation in CsPb(Cl,Br)$_3$ perovskite nanocrystals in a glass matrix, Nano Lett. **22**, 4583 (2022).

[24] Y. Chen, G. H. Li, Z. M. Zhu, H. X. Han, Z. P. Wang, W. Zhou, and Z. G. Wang, Photoluminescence studies of type-II self-assembled In$_{0.55}$Al$_{0.45}$As/Al$_{0.5}$Ga$_{0.5}$As quantum dots grown on (311)A GaAs substrate, Appl. Phys. Lett. **76**, 3188 (2000).

[25] D. S. Abramkin, M. A. Putyato, S. A. Budennyy, A. K. Gutakovskii, B. R. Semyagin, V. V. Preobrazhenskii, O. F. Kolomys, V. V. Strelchuk, and T. S. Shamirzaev, Atomic structure and energy spectrum of Ga(As,P)/GaP heterostructures, J. Appl. Phys. **112**, 083713 (2012).

[26] D. Scalbert, J. Cernogora, C. Benoit àla Guillaume, M. Maaref, F. F. Charfi, and R. Planel, Nature of the lowest electron states in short period GaAs-AlAs superlattices of type II, Solid State Commun. **70**, 945 (1989).

[27] E. L. Ivchenko, V. P. Kochereshko, A. Y. Naumov, I. N. Uraltsev, and P. Lavallard, Magnetic-field-effects on photoluminescence polarization in type II GaAs/AlAs superlattices, Superlattices Microstruct. **10**, 497 (1991).

[28] R. I. Dzhioev, H. M. Gibbs, E. L. Ivchenko, G. Khitrova, V. L. Korenev, M. N. Tkachuk, and B. P. Zakharchenya, Determination of interface preference by observation of linear-to-circular polarization conversion under optical orientation of excitons in type-II GaAs/AlAs superlattices, Phys. Rev. B **56**, 13405 (1997).

[29] T. S. Shamirzaev, J. Debus, D. R. Yakovlev, M. M. Glazov, E. L. Ivchenko, and M. Bayer, Dynamics of exciton recombination in strong magnetic fields in ultrathin GaAs/AlAs quantum wells with indirect band gap and type-II band alignment, Phys. Rev. B **94**, 045411 (2016).

[30] T. S. Shamirzaev, A. V. Nenashev, A. K. Gutakovskii, A. K. Kalagin, K. S. Zhuravlev, M. Larsson, and P. O. Holtz, Atomic

and energy structure of InAs/AlAs quantum dots, Phys. Rev. B **78**, 085323 (2008).

[31] J. Rautert, T. S. Shamirzaev, S. V. Nekrasov, D. R. Yakovlev, P. Klenovský, Yu. G. Kusrayev, and M. Bayer, Optical orientation and alignment of excitons in direct and indirect band gap (In,Al)As/AlAs quantum dots with type-I band alignment, Phys. Rev. B **99**, 195411 (2019).

[32] T. S. Shamirzaev, A. V. Shumilin, D. S. Smirnov, D. Kudlacik, S. V. Nekrasov, Yu. G. Kusrayev, D. R. Yakovlev, and M. Bayer, Optical orientation of excitons in a longitudinal magnetic field in indirect-band-gap (In,Al)As/AlAs quantum dots with type-I band alignment, Nanomaterials **13**, 729 (2023).

[33] T. S. Shamirzaev, D. S. Abramkin, A. K. Gutakovskii, and M. A. Putyato, High quality relaxed GaAs quantum dots in GaP matrix, Appl. Phys. Lett. **97**, 023108 (2010).

[34] D. S. Abramkin, K. M. Rumynin, A. K. Bakarov, D. A. Kolotovkina, A. K. Gutakovskii, and T. S. Shamirzaev, Quantum dots formed in InSb/AlAs and AlSb/AlAs heterostructures, JETP Lett. **103**, 692 (2016).

[35] A. Chellu, J. Hilska, J.-P. Penttinen, and T. Hakkarainen, Highly uniform GaSb quantum dots with indirect-direct bandgap crossover at telecom range, APL Mater **9**, 051116 (2021).

[36] T. S. Shamirzaev, D. R. Yakovlev, N. E. Kopteva, D. Kudlacik, M. M. Glazov, A. G. Krechetov, A. K. Gutakovskii, and M. Bayer, Spin dynamics of charged excitons in ultrathin (In,Al)(Sb,As)/AlAs and Al(Sb,As)/AlAs quantum wells with an indirect band gap, Phys. Rev. B **106**, 075407 (2022).

[37] T. S. Shamirzaev, D. R. Yakovlev, A. K. Bakarov, N. E. Kopteva, D. Kudlacik, A. K. Gutakovskii, and M. Bayer, Recombination and spin dynamics of excitons in thin (Ga,Al)(Sb,As)/AlAs quantum wells with an indirect band gap and type-I band alignment, Phys. Rev. B **102**, 165423 (2020).

[38] I. A. Merkulov, A. L. Efros, and M. Rosen, Electron spin relaxation by nuclei in semiconductor quantum dots, Phys. Rev. B **65**, 205309 (2002).

[39] A. V. Khaetskii, D. Loss, and L. Glazman, Electron spin decoherence in quantum dots due to interaction with nuclei, Phys. Rev. Lett. **88**, 186802 (2002).

[40] Y. G. Semenov and K. W. Kim, Effect of an external magnetic field on electron-spin dephasing induced by hyperfine interaction in quantum dots, Phys. Rev. B **67**, 073301 (2003).

[41] D. S. Smirnov, E. A. Zhukov, E. Kirstein, D. R. Yakovlev, D. Reuter, A. D. Wieck, M. Bayer, A. Greilich, and M. M. Glazov, Theory of spin inertia in singly charged quantum dots, Phys. Rev. B **98**, 125306 (2018).

[42] E. A. Zhukov, E. Kirstein, D. S. Smirnov, D. R. Yakovlev, M. M. Glazov, D. Reuter, A. D. Wieck, M. Bayer, and

A. Greilich, Spin inertia of resident and photoexcited carriers in singly charged quantum dots, Phys. Rev. B **98**, 121304(R) (2018).

[43] Y. Fu, M. Willander, E. L. Ivchenko, and A. A. Kiselev, Valley mixing in GaAs/AlAs multilayer structures in the effective-mass method, Phys. Rev. B **47**, 13498 (1993).

[44] L. D. Landau and E. M. Lifshitz, *The Classical Theory of Fields*, Course of Theoretical Physics Vol. 2, 4th ed. (Butterworth-Heinemann, Heidelberg, 1994), p. 130.

[45] M. M. Glazov, *Electron & Nuclear Spin Dynamics in Semiconductor Nanostructures* (Oxford University Press, Oxford, 2018).

[46] T. S. Shamirzaev, A. M. Gilinsky, A. K. Bakarov, A. I. Toropov, D. A. Tenne, K. S. Zhuravlev, C. von Borczyskowski, and D. R. T. Zahn, Millisecond photoluminescence kinetics in a system of direct-bandgap InAs quantum dots in an AlAs matrix, JETP Lett. **77**, 389 (2003).

[47] A. V. Shchepetilnikov, D. D. Frolov, Yu. A. Nefyodov, I. V. Kukushkin, D. S. Smirnov, L. Tiemann, C. Reichl, W. Dietsche, and W. Wegscheider, Nuclear magnetic resonance and nuclear spin relaxation in AlAs quantum well probed by ESR, Phys. Rev. B **94**, 241302(R) (2016).

[48] I. D. Avdeev and D. S. Smirnov, Hyperfine interaction in atomically thin transition metal dichalcogenides, Nanoscale Adv. **1**, 2624 (2019).

[49] D. S. Smirnov, T. S. Shamirzaev, D. R. Yakovlev, and M. Bayer, Dynamic polarization of electron spins interacting with nuclei in semiconductor nanostructures, Phys. Rev. Lett. **125**, 156801 (2020).

[50] T. S. Shamirzaev, A. V. Shumilin, D. S. Smirnov, J. Rautert, D. R. Yakovlev, and M. Bayer, Dynamic polarization of electron spins in indirect band gap (In,Al)As/AlAs quantum dots in a weak magnetic field: Experiment and theory, Phys. Rev. B **104**, 115405 (2021).

[51] M. Yu. Petrov, I. V. Ignatiev, S. V. Poltavtsev, A. Greilich, A. Bauschulte, D. R. Yakovlev, and M. Bayer, Effect of thermal annealing on the hyperfine interaction in InAs/GaAs quantum dots, Phys. Rev. B **78**, 045315 (2008).

[52] D. S. Smirnov, E. A. Zhukov, D. R. Yakovlev, E. Kirstein, M. Bayer, and A. Greilich, Spin polarization recovery and Hanle effect for charge carriers interacting with nuclear spins in semiconductors, Phys. Rev. B **102**, 235413 (2020).

[53] G. E. Pikus and F. G. Pikus, The mechanism of heavy and light hole mixing in GaAs/AlAs superlattices, Solid State Commun. **89**, 319 (1994).

[54] G. L. Bir and G. E. Pikus, *Symmetry and Deformation Effects in Semiconductors* (Nauka, Moscow, 1972).